Manuscript prepared for The Cryosphere Discuss.
with version 3.5 of the LaTeX class copernicus_discussions.cls.
Date: 3 May 2013

Antarctic ice-mass balance 2002 to 2012: regional re-analysis of GRACE satellite gravimetry measurements with improved estimate of glacial-isostatic adjustment based on GPS uplift rates

Ingo Sasgen[1], **Hannes Konrad**[1], **Erik R. Ivins**[2], **Michiel R. van den Broeke**[3], **Jonathan L. Bamber**[4], **Zdeněk Martinec**[5], **and Volker Klemann**[1,6]

[1]Department of Geodesy and Remote Sensing, GFZ German Research Centre for Geosciences, Telegrafenberg A20, D-14473, Potsdam, Germany.
[2]Jet Propulsion Laboratory, California Institute of Technology, Pasadena, CA 91109-8099, USA.
[3]Institute for Marine and Atmospheric Research, Utrecht University, 3508 TA Utrecht, The Netherlands.
[4]School of Geographical Sciences, University of Bristol, University Road, Bristol BS8 1SS, United Kingdom.
[5]School of Cosmic Physics, Dublin Institute for Advanced Studies, 5 Merrion Square, Dublin 4, Ireland.
[6]*now at* National Oceanography Centre, 6 Brownlow Street, Liverpool L3 5DA, United Kingdom.

Correspondence to: Ingo Sasgen
(sasgen@gfz-potsdam.de)

Abstract

We present regional-scale mass balances for 25 drainage basins of the Antarctic Ice Sheet (AIS) from satellite observations of the Gravity and Climate Experiment (GRACE) for time period January 2003 to September 2012. Satellite gravimetry estimates of the AIS mass balance are strongly influenced by mass movement in the Earth interior caused by ice advance and retreat during the last glacial cycle. Here, we develop an improved glacial-isostatic adjustment (GIA) estimate for Antarctica using newly available GPS uplift rates, allowing us to more accurately separate GIA-induced trends in the GRACE gravity fields from those caused by current imbalances of the AIS. Our revised GIA estimate is considerably lower than previous predictions, yielding an estimate of apparent mass change of 53±18 Gt/yr. Therefore, our AIS mass balance of -114±23 Gt/yr is less negative than previous GRACE estimates. The Northern Antarctic Peninsula and the Amundsen Sea Sector exhibit the largest mass loss (-26±3 Gt/yr and -127±7 Gt/yr, respectively). A30 In contrast, East Antarctica exhibits a slightly positive mass balance (26±13 Gt/yr), which is, however, mostly the consequence of compensating mass anomalies in Dronning Maud and Enderby Land (positive) and Wilkes and George V Land (negative) due to interannual accumulation variations. In total, 6 % of the area constitutes about half the AIS imbalance, contributing 151±7 Gt/yr to global mean sea-level change. Most of this imbalance is caused by ice-dynamic speed up expected to prevail in the near future.

1 Introduction

The current mass balance of the Antarctic Ice Sheet (AIS), and its response to a changing global climate, is challenging to assess due to the spatio-temporal gaps in the meteorological and glaciological instrumental records. Although satellite measurements have considerably improved our knowledge on the state of the AIS, estimating an accurate mass balance and associated contribution to global sea-level change is difficult due to incomplete spatial coverage of the data sets, and/or the diverse processes influencing the satellite measurements. For example, surface-elevation trends of the AIS acquired with laser or radar altimeters need to

be corrected for the spatially and temporally heterogenous firn compaction (e.g. Helsen et al., 2008) to infer mass trends. The input-output method (e.g. Rignot et al., 2008; Joughin et al., 2010; Rignot et al., 2011) also relies on estimates of the surface velocity and ice thickness close to the grounding line of variable quality. A10 There also may be a bias in the extrapolation to areas of relatively poor data (Rignot, 2008), and there is some uncertainty in converting surface velocity to depth-averaged velocity.

While determining mass trends comparably directly from satellite gravimetry data of the Gravity and Climate Experiment (GRACE) has substantial advantages over other measurements the accuracy of AIS mass balances from GRACE has been limited by a poorly constrained glacial-isostatic adjustment (GIA). The change in volume and extent of the AIS during the last glacial cycle(s) imposed a varying load on the Earth surface, inducing mass movement and surface deformation. Since the mantle material acts as a highly viscous fluid on these millennial time scales, the GIA of the Earth is delayed with respect to the forcing, where the induced response is governed by the viscosity of the Earth's mantle and the temporal evolution of the ice sheet. Despite the major ice retreat associated with the last glacial cycle has ceased in Antarctica, GIA continues, causing an inflow of mantle material and an upward bending of the lithosphere in large areas of the former glacial loads. A12 In the periphery of the ice sheet or in areas with comparably recent accumulation increase, also subsidence may occur due to the collapse of the peripheral forebulge and ongoing adjustment to additionally imposed ice loads, e.g. in East Antarctica (Ivins and James, 2005; Whitehouse et al., 2012b; Ivins et al., 2013); a rather complex GIA pattern is expected that very much depends on the poorly-known lithosphere and mantle structure beneath the AIS. Nevertheless, GIA-induced trends in the Earth's gravity field and in the surface deformation are more and more clearly revealed in Antarctica by space-geodetic observing systems, such as GRACE and GPS, respectively.

Several glacial reconstructions have been proposed for predicting GIA using viscoelastic Earth models. These are based on geomorphologic constraints on the past ice height and extent (e.g., Ivins and James, 2005), thermomechanical ice sheet modeling (e.g., Huybrechts, 2002; Ritz et al., 2001), and – considering GIA-induced surface deformation and gravity field changes of the Earth – on indicators of the past relative sea level (e.g., Lambeck and Chappell, 2001;

Peltier, 2004), as well as a combination of these approaches (e.g. Bassett et al., 2007; Whitehouse et al., 2012a,b). However, due to the sparsity of constraints on the ice sheet evolution during the last glacial cycle, both in space and time, the ambiguity introduced by the poorly known mantle viscosity beneath Antarctica, and the complexity of the ice-dynamic processes involved, the reconstructions and associated GIA predictions substantially differ in their magnitude and spatial pattern, causing a large uncertainty in the mass balance estimates from GRACE (e.g. Barletta et al., 2008; Chen et al., 2009; Thomas et al., 2011).

A13 In this context, GPS uplift rates in Antarctica are an important constraint on GIA. Records of surface deformation dating back to the late 1990's are available from stations of the International GNSS Service (IGS), located near research stations along the coast of Antarctica. Inland stations began to be deployed only after Austral spring of 1995 (e.g. Raymond et al., 2004). The analysis of GPS data now collected are beginning to provide a robust complement to the longer IGS time-series (Thomas et al., 2011), as they bound – although with larger uncertainty due to shorter records – GIA in regions where the signal is expected to be large. Currently, however, the longest, and hence most precise, GPS records remain along the coastal perimeter.

A14 In addition to GPS, also GRACE may represent a constraint on GIA in certain areas of Antarctica. During the last glacial cycle, the dominant amount of ice mass retreated from the major ice-shelf areas, inducing a peak GIA signal in the gravity field. At the same time, contemporary ice-mass variations of and on floating ice shelves can be considered 'transparent' in the GRACE data, as the floating ice freely seeks a freeboard height ocean-ward of the grounding line. Nevertheless, the reliability of the GRACE estimate on Antarctic GIA remains limited due to superposition with the signal from continental ice-mass changes or trends in the ocean beneath the ice shelves.

The aim of the following investigation is to provide more accurate regional mass balances of the AIS based on an improved correction for GIA. We develop this improved GIA estimate by rigorous analysis of available space-geodetic measurements that measure the unique signal standout of the process itself. Although our approach resembles the global inversion of GRACE and GPS data presented by Wu et al. (2010), it includes more accurate and spatially

dense data regionally. Furthermore, here we base the inversion on a richer ensemble of GIA forward models. A15 It also differs from the approach followed by Ivins and James (2005), Whitehouse et al. (2012b) and Ivins et al. (2013), which is based on selecting from a suite of GIA scenarios those that fit geologic and relative sea level constraints and – in the case of the W12a modification (Whitehouse et al., 2012b) in the southern AP, GPS uplift rates, without attempting to formally minimize the misfits to both space gravimetry and terrestrial GPS data. In contrast to the approach of Riva et al. (2009), altimetry data is not used in our inversion due to the persisting problema of relating surface-elevation trends to mass trends. A28a Unless stated otherwise, all GRACE mass balance and acceleration values provided represent error-weighted means with 2-sigma uncertainties for the results based on the GRACE coefficients CSR RL05 and GFZ RL05 for the time period January 2003 to September 2012.

2 Data and methods

2.1 GRACE filtering and inversion

A2 Here, we use 113 monthly mean solutions of the Earth's gravity field derived from data of the GRACE satellites spanning the time interval August 2002 to September 2012. We adopt the GRACE gravity field solutions of release version 5 (RL05) of the processing centres German Research Centre for Geosciences GFZ, Potsdam, Germany (GFZ RL05; Flechtner, 2007), and the Centre for Space Research at University of Texas, Austin, USA (CSR RL05; Bettadpur, 2007), which are publicly available as Stokes potential coefficients complete to degree and order 90 and 60, respectively, at http://isdc.gfz-potsdam.de/. Following the recommendation Bettadpur (2007), the poorly determined GRACE coefficient of degree 2 and order 0 is replaced in CSR RL05 by an estimate from satellite laser ranging (SLR; Cheng and Tapley, 2004), whereas the degree 1 coefficients are completed with estimates from SLR tracking (Cheng et al., 2010), accessible via http://grace.jpl.nasa.gov/data/degree1/. It should be stated that global GPS data is involved in the SLR-based determination of the degree 1 coefficients, due to the sparse and inhomogeneous coverage of SLR tracking stations.

A2 In this paper, we apply the band-pass filtering function presented in Sasgen et al. (2012a), and the coefficients of the forward model, to regionalize the representation of the gravity field and reduce noise in the uncertain low- and high degree and order coefficients (see supplementary material). Barletta et al. (2012) have shown a considerable influence of the current mass loss trends (and accelerations) in Greenland on the degree 1 coefficients. The dominant trend, however, is caused by GIA in North America, causing a geocenter motion rate between 0.1 and 1 mm/yr, depending on the mantle viscosity and the glacial history (Klemann and Martinec, 2011). Considering that observational estimates for the degree 1 coefficients are uncertain and show large deviations between difference methods (e.g. Barletta et al., 2012), we confine the adjustment to coefficients of degree and order 2 to 60. The geocenter motion velocity of the adjusted forward model, however, is shown to agree with the SLR estimate by Cheng et al. (2010) (see supplementary material).

C3a The temporal variations in the gravity field are inverted for mass changes of the AIS using the forward modelling approach detailed in Sasgen et al. (2010) (Appendix A). A16 *A priori*, this involves the calculation of the gravity field changes induced by a prescribed mass distribution within 25 drainage basins (Figure 1); here, surface-ice velocity fields based used for the input-output method (IOM; Rignot et al., 2008) are considered as an indication of where mass changes should be expected, assuming that recent imbalances primarily occur in regions of fast glacier flow. The main effect is that mass changes are concentrated along the margin of the ice sheet, which is a more realistic approximation for ice-dynamic, as well as accumulation-driven mass imbalances than assuming a uniform mass distribution within each basin. The forward model is then regionally adjusted by the method of least squares to fit the GRACE observations. The inversion method is similar to the one used by Schrama and Wouters (2011) in the sense that a modelled signal is fit to the spatial GRACE monthly solutions. The inversion results are weakly dependent on the definition of a priori mass distribution and accurate to $<$10% (Sasgen et al., 2012b).

To isolate present-day ice-mass change and GIA in the GRACE time series we follow a two step procedure. First, we estimate the temporal linear trends in the GRACE gravity fields for the time interval January 2003 to September 2012. We then perform a first-order global-scale inver-

sion of the peak trend signals in the GRACE data using forward models consisting of 35 components (see Supplement Fig. 5); i) present-day ice-mass changes in Greenland (eight basins), Ellesmere Island, Alaska and the Antarctica (25 basins), as well as ii) GIA over North America and Antarctica . The forward models of i) are based on ICESat surface-elevation changes (Sørensen et al., 2011, Greenland;), airborne laser measurement (Arendt et al., 2002, Alaska;) and surface-ice velocities measured by radar for Antarctica (Rignot et al., 2008). A17 The GIA predictions for the Northern Hemisphere are obtained by using a viscoelastic Earth model with a load given by the glacial reconstruction NAWI (Zweck and Huybrechts, 2005). For Antarctica, three different load models and four different viscosity distributions are used (see Table 1). Although the quality of the glacial reconstruction NAWI has not been assessed with, for example, paleo sea-level indicators in the near-field of the ice sheet, it has the advantage of being mostly independent of assumptions on the viscosity distribution. Both the total sea-level variation during the last glacial cycle and the GIA signal over North America are constrained at a sufficiently accurate level (Sasgen et al., 2012b) for isolating and removing this influence on time-varying geoid-heights and crustal displacements in Antarctica. The parameter estimate for the Antarctic GIA signal resulting from the first-order global inversion of the GRACE data is later combined with the estimates based on GPS uplift rates.

2.2 GPS data

The GPS uplift rates used in our study are those presented and provided by Thomas et al. (2011). The rates are obtained from time series of vertical motion, with the time span varying from station to station, the longest being from the year 1995 to 2010. We use the two sets of elastic corrections provided in Thomas et al. (2011), which are based on mass balance estimates from the IOM and ice-mass trends derived from ICESat satellite laser altimetry. Although, Shepherd et al. (2012) showed that mass balance estimates from both methods agree within their uncertainty for large-scale averages over the AIS, results are divergent for regional to local scales; the elastic correction differs up to about $\pm$ 1.5 mm/yr, particularly over the FRIS region and EA. Another problem arises, because the elastic correction rates from IOM and ICESat are not based on the same time span as the GPS uplift rates, giving concerns about an inconsistently

reflecting interannual accumulation-driven elastic deformation. Nevertheless, we consider the IOM method, which contrasts the average accumulation between 1980 to 2004 with the glacial discharge in 2006 (Rignot et al., 2008), to be most appropriate for correcting the long-term GPS records for the elastic deformation. The ICESat-based elastic deformation provided is applied as an alternative correction to capture some of the uncertainty related to contemporary mass variations.

A18 The GPS stations of the northern Antarctic Peninsula (OHI2, ROTB and PALM) tend to exhibit a kink in the time series of the vertical component after the Larsen Ice Shelf breakup in 2001 (Thomas et al., 2011). Here, we include estimates of the vertical motions for these stations prior to the breakup event of 2002, though the crustal motion is likely to be a mixture of viscous and elastic responses that have memory of the losses prior to 2002 (Rignot et al., 2005). The complexity of the response is exacerbated by the quite low asthenospheric viscosity that occurs in mantle adjacent to the Bransfield Strait and a young mantle slab window Ivins et al. (2011); Simms et al. (2012); Nield et al. (2012). Also, for SMRT, only GPS uplift rates prior to 2002 are included, despite the fact that the station record does not exhibit a significant change of the trend from 2002 until ceasing measurement in early 2005 (Thomas et al., 2011). We thus include 46 GPS estimates of uplift rates for 35 mostly near-coastal locations along with their uncertainties as a new constraint on GIA. A23 We assume uncorrelated errors, also for co-located GPS sites, despite the GPS processing may rely on the same clock and orbit estimates causing correlated station estimates. The GPS uplift rates are corrected for surface deformation arising from the Northern Hemisphere GIA (and present-day ice-mass balance in Alaska, Greenland and Ellesmere Island) that are related to two effects; i) a shift of the centre of figure with respect to the centre of mass of the Earth, in which the GPS data are supplied, as well as changes in the Earths rotation, and ii) surface deformation caused by the uplift of all continents by the ocean loading since the Last Glacial Maximum. A19 Using the first-order global inversion estimate from GRACE, we estimate this correction to amount 0.03 ± 0.08 mm/yr at the location of the GPS stations.

3 Improved estimate of Antarctic glacial-isostatic adjustment

In the following, we will distinguish between a GIA prediction – obtained by applying a glacial reconstruction to a viscoelastic Earth model assuming a set of Earth model parameters, and a GIA estimate – obtained by inversion of (space-)geodetic measurements. In this sense, the load histories of Ivins and James (2005), Huybrechts (2002) and Peltier (2004) are glacial reconstructions, and the associated present-day Earth response is a GIA prediction. In contrast, the GIA signals inferred by Riva et al. (2009) (Antarctica; from ICESat and GRACE) and Wu et al. (2010) (global; from GPS and GRACE) are considered GIA estimates. Whitehouse et al. (2012a) performed extensive GIA modelling to derive an Antarctic glacial reconstruction validated, in part, with present-day measurements (Whitehouse et al., 2012b). These results can be considered a GIA formal prediction. It should be emphasized that we do not attempt to evaluate the glacial histories our GIA predictions are based upon. A20 But we aim at providing a new empirical estimate of Antarctic GIA along with its uncertainties hereinafter called the Antarctic glacial-isostatic adjustment estimate version 1 (AGE1). B4 Due to a broader sampling of the parameter space compared to Wu et al. (2010), AGE1 is more independent from assumptions on the viscosity distribution or glacial reconstruction taken there. However, it still relies on three roughly similar glacial reconstructions (not including all geomorphological data available today) and a limited range of mantle viscosity distributions; including regional advance and retreat scenarios, which are not captured by the glacial histories, or a more complex rheological structure underneath Antarctica, such as a ductile crustal layer (e.g. Schotman and Vermeersen, 2005), may influence the resulting AGE1 GIA estimate and its uncertainty range. Nevertheless, AGE1 represents an GIA estimate, alternative to the predictions of Ivins and James (2005) or Whitehouse et al. (2012a), for correcting GPS, GRACE and altimetry trends in Antarctica.

3.1 Modelling of the GIA in Antarctica

We predict GIA with the viscoelastic Earth model of Martinec (2000), which solves the governing equations of a Maxwell-viscoelastic continuum with the spectral-finite element approach and an explicit time scheme. Rotational deformation is implemented, as well as the sea-level

equation, allowing for the migration of coastlines (Hagedoorn et al., 2007). Here, the Earth model is run with spatial resolutions of spherical-harmonic degree and order 170 (equivalent to 118 km). As free parameters of the model, we consider the viscosity of the upper and lower mantle, η_{UM} and η_{LM}, respectively, as well as the thickness of the elastic lithosphere h_{L}.

We force our viscoelastic Earth model with three load histories, derived from three published glacial reconstructions of the AIS, LH1 (after Huybrechts, 2002, version digitized from publication), LH2 (after Peltier, 2004, publicly avaliable) and LH3 (after Ivins and James, 2005, *pers. comm.*). For LH2, the maximum ice height of the disc-shaped loading centered at the pole was reduced from 765 m to 444 m, to obtain a smooth transition to neighboring regions. To obtain regional retreat histories, we subdivide the AIS into five sectors (see Fig. 1 in supplement); Antarctic Peninsula (AP), Filchner-Ronne Ice Shelf (FRIS), Ross Ice Shelf (RIS), Amery Ice Shelf (AMIS) and the remaining parts, East Antarctica (EAIS). The criteria for the division are 1) to capture areas with substantial ice retreat in all load histories LH1, LH2 and LH3, and to encompass the main clusters of GPS stations recording the regional GIA signals. That is 6 stations in AP, 14 in FRIS, 13 in RIS, 4 in AMIS, and 9 in EAIS . We then predict the global GIA-induced rate of radial displacement, u_r (in centre of figure), and rate of geoid-height change, e_r (in centre of mass), subject to the forcing of each per-sector subdivision ($r = 1$ through 5, corresponding to AP, FRIS, RIS, AMIS and remaining parts, EAIS) of each load history LH1, LH2 and LH3. B5b The calculation is repeated for each per-sector load history adopting four different radial-symmetric viscosity distributions VD1 through VD4 (Table 1). The thickness of the elastic lithosphere is held constant at 100 km, except for EAIS (150 km) and A21a AP (60 km), where seismic tomography suggest considerably greater and lesser lithosphere thicknesses, respectively (Danesi and Morelli, 2001; Kobayashi and Zhao, 2004), A21c even though there is evidence for a thinner lithosphere in AP (Yegorova et al., 2011).

3.2 GRACE and GPS as a constraint on GIA

We estimate GIA-induced fields of e and u for entire Antarctica from the GRACE and GPS data, respectively, by linear combination of GIA signal caused by the per-sector loading history (LH1, LH2 and LH3) and viscosity distribution (VD1 through VD4). This is done, by

estimating a scalar parameters S_r from the fitting of either geoid rates to GRACE observations (S_r^{GRACE}; result from inversion step 1 described above), displacement rates to GPS (S_r^{GPS}) or both simultaneously ($S_r^{\mathrm{comb.}}$),

$$e_{\mathrm{Total}}(\mathbf{\Omega}) = \sum_r S_r \cdot e_r(\mathbf{\Omega}), u_{\mathrm{Total}}(\mathbf{\Omega}) = \sum_r S_r \cdot u_r(\mathbf{\Omega}), \tag{1}$$

where $\mathbf{\Omega}$ stands for the spherical colatitude ϑ and longitude φ, hence, $\mathbf{\Omega} = (\vartheta, \varphi)$. Here, we adopt a global solution domain, $0^{\mathrm{o}} \leq \vartheta \leq 90^{\mathrm{o}}$, $-180^{\mathrm{o}} \leq \varphi \leq 180^{\mathrm{o}}$. The scalar parameter S_r can be interpreted as adjustment factors on the ice heights of the glacial reconstruction due to the approximate linearity of the GIA response with respect to the forcing. It is estimated by minimizing the difference between the predicted and observed fields of e and u in the least-squares sense. B7a For the GRACE-based estimate, a single scaling factor is derived, S^{GRACE} such that the GIA-induced rate of geoid-height change fits the GRACE trends over a latitude- and longitude-limited adjustment area centred over the Filchner-Ronne ice shelf, which is then applied to all other sectors. The intention of the GRACE constraint is to i) compensate for the changes in the GIA magnitude due to different viscosity profiles, and, later in the combined adjustment with the GPS data to ii) constrain the regional fit to the GPS data to remain near the GRACE-scaled GIA prediction. For the GPS-based estimate, we estimate five scaling parameters simultaneously, S_r^{GPS}, meaning that the proportion between the per-sector load history in LH1, LH2 and LH3 may change. The parameters are obtained by minimizing the misfit between observed and modelled uplift rates at the location of the GPS stations, $u_{\mathrm{Total}}(\mathbf{\Omega}_i)$ and $u_{\mathrm{obs.}}(\mathbf{\Omega}_i)$, respectively, $i = 1$ through 46. A22 It is worth noting that the method effectively results in non-physical ice sheet representation at the boundaries of the sectors; that is jumps in the ice thickness, which are, however, of minor importance because of the elastic lithosphere acting as an effective low-pass filter.

The GIA-estimate satisfying both GRACE and GPS observations according to their respective errors, is obtained by the constrained least-squares approach (e.g. Tarantola, 2005). This approach provides a parameter estimate under the condition that it is close to an *a priori* value – the deviation being governed by the balance of the uncertainties of the data and the *a priori*

parameter (constraint). B5a Here, the *a priori* value is the scaling factor, B7b $\mathbf{S}^{\mathrm{GRACE}}$, derived from the GRACE signal over the FRIS sector. It is calculated for each load history and viscosity distribution and then applied, assuming that the spatial pattern of LH1, LH2, and LH3 is correct, to the GIA signal of the remaining sectors. Based on the constrained (GRACE&GPS) or unconstrained (GPS only) parameter estimate, S_r^{GPS} and $\mathbf{S}^{\mathrm{comb.}}$, respectively, five per-sector fields $e_r(\mathbf{\Omega})$ and $u_r(\mathbf{\Omega})$ are scaled and summed up for each of the 12 combinations of load history and viscosity distribution, leading to a GIA estimate for entire Antarctica according to Equation (1) A24a C3c,

$$\begin{aligned}\mathbf{S}^{\mathrm{comb.}} =& \mathbf{S}^{\mathrm{GRACE}} + \left(F^{\mathrm{T}} C_{\mathrm{GPS}}^{-1} F + C_{\mathrm{GRACE}^{-1}}\right)^{-1} \\ & \cdot F^{\mathrm{T}} C_{\mathrm{GPS}}^{-1} \left(\mathbf{u}_{\mathrm{obs}} - F\,\mathbf{S}^{\mathrm{GRACE}}\right) ,\end{aligned} \tag{2}$$

where the symbols are as follows:

$\mathbf{S}^{\mathrm{comb.}}$	$= (S_1^{\mathrm{comb.}},...,S_5^{\mathrm{comb.}})^{\mathrm{T}}$
$\mathbf{S}^{\mathrm{GRACE}}$	$= (S_1^{\mathrm{GRACE}},...,S_5^{\mathrm{GRACE}})^{\mathrm{T}}$
F_{ir}	$= u_r(\mathbf{\Omega}_i)$ (design matrix)
C_{GRACE}	covariance matrix of $\mathbf{S}^{\mathrm{GRACE}}$
C_{GPS}	covariance matrix of GPS observations
$\mathbf{u}_{\mathrm{obs.}}$	$= (u_{\mathrm{obs.}}(\mathbf{\Omega}_1),...,u_{\mathrm{obs.}}(\mathbf{\Omega}_{46}))^{\mathrm{T}}$.

A24b The design matrix F contains the GIA-induced uplift rates at the 46 GPS station locations predicted by each of the five per-sector load histories and four viscosity profiles, which is then iterated (see below). A24c B2a It should be noted that although the forcing from each glacial history for AP, FRIS, RIS, AMIS and EAIS is confined by distinct boundaries, the GIA response in surface deformation extends beyond each sector, on the one hand because the elastic lithosphere acts as a low-pass filter, on the other hand because the Earth response produces a peripheral forebulge along the margin of the load change. This implies that the fit of each parameter S_r is influenced also by $u_{\mathrm{obs.}}(\mathbf{\Omega}_i)$ and $u_{\mathrm{Total}}(\mathbf{\Omega}_i)$ in other sectors.

Since the combination of GRACE and GPS observations in the scaling parameter $\mathbf{S}^{\mathrm{comb.}}$ is sensitive to the parameter and data uncertainties, special care has to be taken in estimating

meaningful (co-)variance matrices C_{GRACE} and C_{GPS}. For the scaling factor inferred from GRACE, we estimate errors due to i) A25a leakage of present-day signal by estimating the scaling factor with and without adjusting for contemporary ice-mass changes in basins 4 to 25; a leakage errors is estimated to 29 %), ii) sensitivity w.r.t. the choice of the adjustment area (variability introduced by subdividing the adjustment area in four sectors; 9 %), iii) remaining aliasing periods of oceanic tides underneath the FRIS (A25b with and without estimating S_2 with 161.5 day and K_2 with 1395.7 day periods in temporal decomposition; $< 5\%$), iv) difference between two data sets of GRACE coefficients (GFZ RL05 vs. CSR RL05; 9 %), and v) formal GRACE coefficient uncertainties ($< 2\%$), adding up to a total uncertainty of 32% for S_r. Uncertainties for the GPS trends are taken from (Thomas et al., 2011). The sensitivity of our results to the choice of the GPS and GRACE uncertainties is discussed below.

3.3 Statistical approach to mean GIA estimate

To obtain a robust GIA correction, that is as independent as possible from assumptions on the load history and viscosity distribution, we apply the following statistical approach. We perform the estimation procedure of S_r^{GPS}, and $S_r^{\mathrm{comb.}}$ detailed above while A26 permuting

1. load history (LH1, LH2, LH3) and viscosity distribution (VD1 through VD4) for each sector ($3^5 \cdot 4^5$ possibilities),

2. elastic corrections for GPS uplift rates (2 possibilities; based on input-output method and ICESat) (Thomas et al., 2011),

3. GRACE release (2 possibilities; CSR RL05 and GFZ RL05),

resulting in an ensemble of 995328 samples, where 1) modifies the design matrix F and the GRACE constraint $\mathbf{S}^{\mathrm{GRACE}}$, 2) the GPS observation vector $\mathbf{u}_{\mathrm{obs.}}$ and 3) again the GRACE constraint. The estimates from GPS, S_r^{GPS}, are affected only little by the GRACE release permutation – merely due to subtracting a different estimate of the Northern Hemisphere contribution to the observed GPS uplift rates.

Finally, the apparent rate of ice-mass change is calculated for each basin and the entire AIS from the ensemble of S_r^{GPS} and $S_r^{\mathrm{comb.}}$, which are applied to the apparent ice-mass change associated with the unscaled fields for each sector, load history and viscosity distribution. For each of the three types (GRACE & GPS and GPS) and each of the 995328 samples, the far-field contribution of the Northern Hemisphere GIA and present-day ice mass change is estimated based on the load history and viscosity distribution adopted for the FRIS sector.

3.4 Apparent ice-mass change of GIA correction

The GRACE signal over the FRIS area requires a downward adjustment of the initial GIA predictions mainly for LH1 and LH2, for most combinations of load histories and viscosity distributions, whereas the signal of LH3 already reconciles with GRACE over the FRIS area. In principle, a scaling factor could also be obtained for the RIS area; however, here, we determine only a single factor based on the FRIS, which is intended to compensate for the trade-off between the viscosity distribution and magnitude of the load. This factor is then applied (for a specified viscosity distribution) to all other areas, meaning that the spatial pattern of the GIA signal is entirely governed by the model. Although the adjustment reduces spread for different viscosity distributions for each load history to $<$30 Gt/yr, the differences between load models remains large due to their distinct spatial patterns (90 Gt/yr between minumum and maximum estimate). By the sector-wise adjustment to the GPS uplift rates, the load histories are homogenized, reducing the deviation to 38 Gt/yr.

Figure 3 shows the residuals of the uplift rates at the GPS stations after subtracting GIA estimate (GPS only). For each sector, the distribution of residuals is centered around zero (standard deviation of 2.7 mm/yr), even though for FRIS there is an indication that the subtracted GIA is slightly underestimated. The apparent mass change associated with this GIA correction is 50$\pm$26 Gt/yr. For the GIA estimate constrained by GRACE& GPS, the GIA estimate increases in magnitude to 53$\pm$18 Gt/yr. The mean bias slightly increases (-0.1 mm/yr), but GPS uplift residuals for the stations in the FRIS and AMIS center slightly better around zero. This is an indication that GRACE-constrained GIA estimate reproduces data better, which have have short records, uncertain trends, and are given a low weight in the GPS-only adjustment (Figure 2). In

general, the fit to the GPS uplift rates is dominated by the long-term, and hence, most accurate station records. B2c Due to the comparably large error of the GRACE-based scaling factor (32%), the contribution to the combined estimate is small, and GPS and GRACE&GPS (Figure 4). A11 A21b It should be noted that varying the lithosphere thickness also influences the pattern of the regional GIA signals, particularly in the peripheral region of the former ice sheet, and, therefore, may also affect the fit to individual GPS stations. It is expected, however, that after scaling, this will mainly influence the spread of the GPS uplift residuals and apparent mass change values, not so much their mean.

C3b Figure 4 shows the distributions of the GIA-induced apparent mass change for each of the 25 drainage basins of the AIS and the total AIS for GIA estimate AGE1 (GPS & GRACE comb.). Largest GIA-induced mass change is obtained for the basins in the vicinity of the large ice shelves; 4 to 6 Gt/yr for basins 17, 18 and 19 (RIS) and basins 1 and 3, as well as 4 Gt/yr basin 2 and for the southern part of AP (basin 24). A1 For many basins, the scatter of the values are similar to a Gaussian distribution. A5 But since sub-sector GIA signal is mostly governed by the shape of the ice histories LH1, LH2 and LH3, systematic clusters appear for some basins (e.g. basin 25 of the AP, basin 16 in East Antarctica) – differences between the load histories, which are small on average for each sector, again become important. It becomes clear that although LH1, LH2 and LH3 include some of the variety obtained of different reconstructions, further regionally refined glaciation histories will alter the GIA pattern and, therefore, the influence basin-scale apparent mass change.

The reader is encouraged to apply the GIA correction directly to the GRACE coefficients. We therefore provide the GIA estimate AGE1 (GPS & GRACE comb. and GPS only) of the rate of geoid-height change and rate of radial displacement as fully normalized spherical-harmonic coefficients (Heiskanen and Moritz, 1967) in the Supplementary Material to this paper.

4 Regional-scale trends and accelerations from GRACE

Table 2 presents rates and accelerations of mass changes for the 25 basins of the AIS from GRACE A28b for the time period January 2003 to September 2012. The mass balance of the

AIS is characterized by strong losses along the Antarctic Peninsula and Amundsen Sea sector (-140±16 Gt/yr; basins 1, and 18 to 25) and moderate gain of mass for East Antarctica (26±13 Gt/yr; basins 2 to 17), adding up to total of -114±23 Gt/yr. A29 Major mass loss in West Antarctica occurs in basin 21 (Thwaites glacier system; -57±3 Gt/yr) and basin 22 (Pine Island glacier; -28±3 Gt/yr). Mass loss along the Antarctic Peninsula is concentrated in the north, basin 25 (-26±3 Gt/yr). This compares well to GRACE estimates (January 2003 to March 2009) that are slightly higher at -32±6 Gt/yr by (Ivins et al., 2011) and this difference is possibly attributable to a different approach to incorporating the GPS data into the GIA estimation. East Antarctica exhibits a bimodal pattern of mass increase in Dronning Maud and Enderby Land (basins 3 to 8; 60±7 Gt/yr) and mass decrease in Wilkes Land (basins 12 to 15; -31±4 Gt/y).

The situation is more diverse for the acceleration estimates from GRACE presented also in Table 2, A28c here w.r.t. to the mid-point of the time interval January 2003 to September 2012. Acceleration of mass loss (negative in sign) is observed for the Antarctic Peninsula – here, Palmer Land (basin 24; -6±2 Gt/yr^2), as well as for the Amundsen Sea Sector, in particular, the Pine Island, Thwaites and Getz/Hull/Land glacier systems (basins 22, 21 and 20, respectively; -17±6 Gt/yr^2). For the northern Antarctic Peninsula, the acceleration term is not statistically significant. For East Antarctica, mass loss acceleration is observed for Wilkes Land (basin 12; -2±1 Gt/yr^2, while deceleration (positive in sign; decrease of mass loss) is observed in Dronning Maud Land and Enderby Land (basins 4, 5, 6 and 7; 14±4 Gt/yr^2). For the entire AIS, mass loss acceleration arising in West Antarctica (-21±10 Gt/yr^2) is counterbalanced by about half by mass loss deceleration in East Antarctica (12±6 Gt/yr^2), adding up to a total of -16±12 Gt/yr^2.

Figure 5 presents the basin-scale mass balance estimates of the AIS from GRACE (GIA correction AGE1, GRACE&GPS), ordered according to the expected signal-to-noise ratio of present-day ice-mass balance value and the sum of propagated GRACE coefficient errors, filtering and inversion uncertainties, and uncertainties of the GIA correction from Table 2. Additionally, the cumulative sum of the basin-scale mass balances are shown. The most dominant imbalances originate from the northern Antarctic Peninsula (basin 25) and the Amundsen and Bellinghausen Sea Sector (basins 20, 21 and 22). Due to the rather weak influence of our GIA

correction in these basins – A32 B5c which is, however, in contrast to the finding of Groh et al. (2012), who attribute 34±12 Gt/yr to GIA in the Amundsen Sea Sector – and the strong imprint in the GRACE gravity fields, the sum of imbalances amounting to -153 Gt/yr is resolved with an accuracy of ±7 Gt/yr (5%). Representing only 6% of the area of the ice sheet, more than half of the mass imbalances (53%), positive or negative, occurs in these well resolved basins. But even if all increase in mass observed with GRACE is attributed to snow accumulation, and not GIA, the total AIS mass balance remains significantly negative (-61±15). However, mass trends in East Antarctica are strongly influenced by interannual accumulation variability along the coast, limiting the significance of extrapolating the total AIS mass balance into the future.

A31 The acceleration terms inferred for each of the 25 basins for January 2003 to September 2012 are shown in Figure 6, which are ordered identical to the trend estimates depicted in Figure 5 (not according to their signal-to-noise ratio). In West Antarctica, substantive accelerations of mass loss (negative in sign) occurs mainly in the Thwaites (-8±1 Gt/yr^2; basin 21) and the Getz/Hull/Land glacier systems (-6±6 Gt/yr^2; basin 20), and to a lesser extent in the Pine Island glacier (basin 22; -3±1 Gt/yr^2) in the Amundsen Sea Sector. Evidence of glacier retreat and acceleration of ice flow in these regions B12 (Rignot et al., 2011) suggests that the GRACE trends and accelerations reflect long-term responses of the ice sheet, caused by melting of ice shelves by wind-driven penetration of warm ocean water, decreasing buttressing of tributary ice streams (Pritchard et al., 2012). In contrast, for northern Graham Land (basin 25) no statistically significant acceleration is found, despite a strong imbalance in this region. East Antarctica apparently compensates 12±6 Gt/yr^2 of the mass loss acceleration. Here, however, a preliminary comparison with output from the regional atmospheric climate model (RACMO2/ANT Helsen et al., 2008; Lenaerts et al., 2012) suggests that the changes in Dronning Maud Land and Enderby Land (basins 4 to 7; 14±4 Gt/yr^2), Wilkes Land (basins 12 and 13; -4±1 Gt/yr^2), and also those in Palmer Land, Antarctic Peninsula (basin 24; -6±1 Gt/yr^2), are nearly completely explained by accumulation variations within the comparably short observation period.

5 Discussion

Our mass balance for the AIS of -114±23 Gt/yr for the time period January 2003 to September 2012 and our new GIA estimate AGE1 (GPS&GRACE) is considerably less negative than early GRACE estimates of Velicogna (2009) (-143±73 Gt/yr; 2002–2009), who applies a mean GIA correction of 176±76 Gt/yr based on the reconstructions of Ivins and James (2005) and Peltier (2004) and a suite of viscosity distributions. This is mainly a result of correcting GIA with only 53±18 Gt/yr. B10 Our study confirms the estimate -109±48 Gt/yr (Horwath and Dietrich, 2009), based on the shorter time interval August 2002 to January 2008. It also supports the previous joint inversion estimate for the total AIS based on GRACE and GPS data (Wu et al., 2010) of -87±43 Gt/yr (2002-2008), even though with a very different separation between East and West Antarctica – -116±15 Gt/yr and 26±13 Gt/yr (this study) versus -64±32 Gt/yr and -23±29 Gt/yr (Wu et al., 2010), respectively — most likely owing to regional differences between the GIA estimates. And our estimate lies within the range of -87±43 Gt/yr (2000-2011) provided the multi-satellite ice sheet mass balance inter-comparison exercise (IMBIE; Shepherd et al., 2012), using the average of the most recent GIA corrections of Whitehouse et al. (2012b) and Ivins et al. (2013).

B3 Compared to the recent estimate of King et al. (2012) with -69±18 Gt/yr, based on the new GIA prediction W12a (Whitehouse et al., 2012b), our results are with -114±23 Gt/yr significantly more negative, even though excellent agreement is obtained for single glacier systems in the Amundsen Sea, e.g. Thwaites; -57±3 Gt/yr (this study) and -54±5 Gt/yr (King et al., 2012), and Pine Island Glacier; -28±3 Gt/yr (this study) and -24±7 Gt/yr (King et al., 2012). Differences mainly reside in the East Antarctica, for which (King et al., 2012) propose a mass gain of 60±13 with a GIA correction close to zero (3 Gt/yr; W12a model), however, with upper and lower bounds of 56 Gt/yr and -26 Gt/yr, respectively, which also encompass our GIA estimate of 30±11Gt/yr for East Antarctica (Table 2). Without GIA correction, our apparent GRACE mass balance for East Antarctica is 56±7 Gt/yr, in agreement with the 63 Gt/yr provided by King et al. (2012). Possibly, the uncertainty range of W12a in East Antarctica of 82 Gt could be reduced by including GPS uplift rates.

A33 With the GIA-estimate AGE1 (GRACE&GPS), the GRACE indicates a modest mass increase for East Antarctica (26±13 Gt/yr), supporting estimates from radar altimetry 22±39 Gt/yr rather than from the mass budget method -30±76 (Shepherd et al., 2012, October 2002 to December 2008;). However, comparing different time periods is of limited validity due to the strong influence accumulation variations in EA, as discussed above. For the northern Antarctic Peninsula (basin 25) our results of -26±3 Gt/yr show excellent agreement with the most recent GRACE-based estimates of (-33 ± 3 Gt/yr; August 2002 to December 2012 King et al., 2012), and a previous estimate of -32±6 Gt/yr for the time period January 2003 to March 2009 (Ivins et al., 2011).

Compared to other recent GRACE estimates of the AIS mass balance, we obtain stronger losses, even if a similar GIA correction is applied; for example, Ivins et al. (2013) correct for an GIA-induced apparent mass change of 55±13 Gt/yr based on the revised version of Ivins and James (2005) glacial history, resulting in a mass loss of the AIS of -57±34 Gt/yr. Both methods use very different approaches towards regionalizing, as well removing leakage from and to the region of Antarctica. A3 In particular, our treatment of the degree 1 terms is different from Ivins et al. (2013) and the procedure agreed upon in IMBIE (Shepherd et al., 2012); due to the uncertainty of the degree 1 coefficients estimate from SLR and the large influence of far-field signal (e.g. GIA from the Northern Hemisphere), we exclude these coefficients from the *adjustment* of our forward model, which is, however, complete for spherical-harmonic degree and order 0 to 512 (see Supplement). If the predetermined approach used in IMBIE is applied, this may weaken the estimate by about 30 Gt/yr (Ivins et al., 2013).

As shown in Figure 3, AGE1 (GPS&GRACE) fit the GPS uplift rates with a mean bias of -0.1 mm/yr and a standard deviation of 2.2 mm/yr. This is a significant improvement with respect to the bias of -1.2 mm/yr associated with the GIA prediction of (Whitehouse et al., 2012a,b). Due to our statistical approach, AGE1 (combined and GPS-based) is rather insensitive to the viscosity distribution and to the glacial history – at least when integrating over a sector – as deviations are mostly scaled out by the loading adjustment. However, the uncertainty of the GIA correction (Figure 4, suppl.) depends to a large extent on the availability and accuracy of GPS uplift rates. For example, AGE1 suggests the largest GIA anomaly in the RIS sector due to

very sparse GPS data (Figure 3), which is in contrast to more recent geomorphological evidence on the ice sheet retreat in the RIS sector (Ivins et al., 2013). The uncertainties of AGE1 (Figure 4, suppl.) should be kept in mind when applying it as a GIA correction to the GRACE data.

A7 | B2b | B5b Limitations of AGE1 also apply to the representation of the sub-sector (i.e. basin-scale) GIA – arising from unknown regional retreat history. For example, (Groh et al., 2012) presented evidence for a GIA-induced uplift in the Amundsen Sea Sector (part of the FRIS sector in our study) ranging for different locations between 14.1±6.7 and 22.9±6.7 mm/yr, causing a mass increase of 34±12 Gt/yr. These uplift rates are exceptionally large compared to the trends measured by (Thomas et al., 2011), and, if included in our adjustment, can not be fitted by our GIA sectorial patterns; we obtain a GPS residual of 13 to 22 mm/yr for the additional stations, compared to a maximum deviation of 8 mm/yr for the stations of Thomas et al. (2011). Another example is the subsidence due to a substantial ice-thickness increase in the late Holocene predicted by Whitehouse et al. (2012a) in Coats Land (basin 3) of our East Antarctic sector. Clearly, further detailed research on the regional Antarctic GIA signal is needed.

6 Conclusions

We have provided a revised GIA estimate for Antarctica, AGE1, based on numerical simulations and newly available GPS uplift rates, as well as GRACE trends beneath the Filchner-Ronne-Ice shelf. The residual misfit of surface deformation associated with AGE1 (GRACE&GPS) and measured GPS uplift rates in Antarctica is -0.1 mm/yr, which represents an improvement with respect to the GIA prediction e.g. of Whitehouse et al. (2012b) (-1.5 mm/yr mean bias at 46 GPS stations of W12a model, optimum earth model). The apparent ice-mass change of 53±18 Gt/yr associated with AGE1 is considerably lower than previous estimates, in particular, compared to the earlier correction 176±76 Gt/yr applied by Velicogna and Wahr (2006) based on a combination of ICE5G (Peltier, 2004) and IJ05 (Ivins and James, 2005), but in line with more recent, independently derived GIA corrections of Whitehouse et al. (2012b) and Ivins et al. (2013). The implication is significantly weaker negative AIS mass balance of -114±23

Gt/yr estimated from GRACE for the time period January 2003 to September 2012.

Our regional GIA and GRACE mass balance estimates clearly show that more than half of current Antarctic sea-level contribution (positive or negative) arises from 6% of the area of the ice sheet; mass loss along the northern Antarctic Peninsula and the in Amundsen Sea Sector amount to -151±7 Gt/yr. East Antarctica, in contrast, has a slightly positive mass balance (26±12 Gt/yr), exhibiting a bipolar signature of accelerating mass increase in Dronning Maud Land and Enderby Land (basins 5, 6 and 7; 12±4 Gt/yr^2) and accelerating mass loss in Wilkes Land and George V Land (basin 13 and 14; -4±2 Gt/yr^2). The preliminary comparison with output from RACMO2/ANT suggests that the temporal signatures in East Antarctica (and Palmer Land, Antarctic Peninsula) are mainly due to interannual accumulation variability; enhanced precipitation in the years 2005 and 2007 as part of variability in the large scale atmospheric circulation have induced these mass anomalies, not changes in ice-dynamic flow. The strong imbalance and acceleration observed for the northern Antarctic Peninsula and the Amundsen Sea Sector (-151 Gt/yr and -22 Gt/yr^2, respectively), however, clearly reflect more vigorous ice flow (Scambos et al., 2004; Rignot et al., 2008) and are more likely to be a sustained sea-level contribution of AIS.

Acknowledgements. Ingo Sasgen and Hannes Konrad would like to acknowledge support from the Deutsche Forschungsgemeinschaft (DFG, German Research Foundation) through grant SA 1734/2-2 and Volker Klemann through grant KL 2284/1-3 (both SPP1257); IS performed part of this work at the Jet Propulsion Laboratory, California Institute of Technology. We would like to thank the German Space Operations Center (GSOC) of the German Aerospace Center (DLR) for providing continuously and nearly 100% of the raw telemetry data of the twin GRACE satellites. This work is a contribution to the "Helmholtz Climate Initiative REKLIM" (Regional Climate Change), a joint research project of the Helmholtz Association of German research centres (HGF). Michiel van den Broeke acknowledges support from Utrecht University and the Netherlands Polar Programme. ERI is supported by NASA's Earth Surface and Interior Focus Area and Cryosphere Program: work performed at the Jet Propulsion Laboratory, California Institute of Technology. JLB was partly supported by the European Commission's 7th Framework Programme through grant number 226375. Ice2sea contribution number ice2sea137. ZM acknowledges support from the Grant Agency of the Czech Republic through Grant No. P210/10/2227.

References

Arendt, A. A., Echelmeyer, K. A., Harrison, W. D., Lingle, C. S., and Valentine, V. B.: Rapid Wastage of Alaska Glaciers and Their Contribution to Rising Sea Level, Science, 297, 382–386, doi:10.1126/science.1072497, 2002.

Barletta, V. R., Sabadini, R., and Bordoni, A.: Isolating the PGR signal in the GRACE data: impact on mass balance estimates in Antarctica and Greenland, Geophys. J. Int., 172, 18–30, doi:10.1111/j.1365-246X.2007.03630.x, 2008.

Barletta, V. R., Sørensen, L. S., and Forsberg, R.: Variability of mass changes at basin scale for Greenland and Antarctica, The Cryosphere Discussions, 6, 3397–3446, doi:10.5194/tcd-6-3397-2012, 2012.

Bassett, S., Milne, G., Bentley, M., and P. Huybrechts, P.: Modelling Antarctic Sea-Level Observations to Test the Hypothesis of a Dominant Antarctic Contribution to Meltwater Pulse IA, Quat. Sci. Rev., 26, 2113–2127, 2007.

Bettadpur, S.: CSR Level-2 Processing Standards Document for Level-2 Product Release 04, Univ. Texas, Austin, Rev. 3.1, GRACE 327-742 (CSR-GR-03-03), 2007.

Chen, J. L., Wilson, C. R., Blankenship, D., and Tapley, B. D.: Accelerated Antarctic ice loss from satellite gravity measurements, Nature Geosci., 2, 859–862, doi:10.1038/ngeo694, 2009.

Cheng, M. and Tapley, B.: Variations in the Earth's oblateness during the past 28 years, J. Geophys. Res., 109, B0940, doi:doi:10.1029/2004JB003028, 2004.

Cheng, M., Tapley, B., and Ries, J.: Geocenter Variations from Analysis of SLR data, IAG Commission 1 Symposium 2010, Reference Frames for Applications in Geosciences (REFAG2010), Marne-La-Vallee, France, 4-8 October 2010s, 2010.

Danesi, S. and Morelli, A.: Structure of the upper mantle under the Antarctic Plate from surface wave tomography, Geophys. Res. Lett., 28, 4395–4398, 2001.

Flechtner, F.: GFZ Level-2 Processing Standards Document for Level-2 Product Release 04, GeoForschungsZentrum Potsdam, Rev. 1.0, GRACE 327-743 (GR-GFZ-STD-001), 2007.

Groh, A., Ewert, H., Scheinert, M., Fritsche, M., Rülke, A., Richter, A., Rosenau, R., and Dietrich, R.: An investigation of Glacial Isostatic Adjustment over the Amundsen Sea sector, West Antarctica, Global and Planetary Change, 98–99, 45 – 53, doi:10.1016/j.gloplacha.2012.08.001, 2012.

Hagedoorn, J. M., Wolf, D., and Martinec, Z.: An Estimate of Global Mean Sea-level Rise Inferred from Tide-gauge Measurements Using Glacial-isostatic Models Consistent with the Relative Sea-level Record, Pure Appl. Geophys., 164, 791–818, doi:10.1007/s00024-007-0186-7, 2007.

Heiskanen, W. A. and Moritz, H.: Physical Geodesy, W. H. Freeman and C., London, 1967.

Helsen, M. M., van den Broeke, M. R., van de Wal, R. S. W., van de Berg, W. J., van Meijgaard, E., Davis, C. H., Li, Y., and Goodwin, I.: Elevation changes in Antarctica Mainly Determined by Accumulation Variability, Science, 320, 1626–1629, doi:10.1126/science.1153894, 2008.

Horwath, M. and Dietrich, R.: Signal and error in mass change inferences from GRACE: the case of Antarctica, Geophys. J. Int., 177, 849–864, doi:10.1111/j.1365-246X.2009.04139.x, 2009.

Huybrechts, P.: Sea-level Changes at the LGM from Ice-dynamic Reconstructions of the Greenland and Antarctic ice sheets During the Glacial Cycles, Quat. Sci. Rev., 21, 203–231, 2002.

Ivins, E. R. and James, T. S.: Antarctic glacial isostatic adjustment: A new assessment, Antarctic Sci., 17, 541–553, 2005.

Ivins, E. R., Watkins, M. M., Yuan, D., Dietrich, R., Casassa, G., and Rülke, A.: On-land ice loss and glacial isostatic adjustment at the Drake Passage: 2003–2009, J. Geophys. Res., 116, B02 403, doi:10.1029/2010JB007607, 2011.

Ivins, E. R., James, T. S., Wahr, J., Schrama, E. J. O., Landerer, F. W., and Simon, K. M.: Antarctic Contribution to Sea-level Rise Observed by GRACE with Improved GIA Correction, J. Geophys. Res., submitted, 2013.

Joughin, I., Smith, B. E., and Abdalati, W.: Glaciological advances made with interferometric synthetic aperture radar, J. Glaciol., 56, 1026–1042, doi:10.3189/002214311796406158, 2010.

King, M. A., Bingham, R. J., Moore, P., Whitehouse, P. L., Bentley, M. J., and Milne, G. A.: Lower satellite-gravimetry estimates of Antarctic sea-level contribution, Nature, 491, 586–590, doi:10.1038/nature11621, 2012.

Klemann, V. and Martinec, Z.: Contribution of glacial-isostatic adjustment to the geocenter motion, Tectonophysics, 511, 99 – 108, doi:10.1016/j.tecto.2009.08.031, 2011.

Kobayashi, R. and Zhao, D.: Rayleigh-wave group velocity distribution in the Antarctic region, Phys. Earth. Planet. Int., 141, 167–181, doi:10.1016/j.pepi.2003.11.011, 2004.

Lambeck, K. and Chappell, J.: Sea-level change throughout the Last-Glacial Cycle, Science, 292, 679–686, doi:10.1126/science.1059549, 2001.

Lenaerts, J. T. M., van den Broeke, M. R., van de Berg, W. J., van Meijgaard, E., and Kuipers Munneke, P.: A new, high-resolution surface mass balance map of Antarctica (19792010) based on regional atmospheric climate modeling, Geophys. Res. Lett., 39, n/a–n/a, doi:10.1029/2011GL050713, 2012.

Martinec, Z.: Spectral-finite element approach to three-dimensional viscoelastic relaxation in a spherical earth, Geophys. J. Int., 142, 117–141, 2000.

Nield, G. A., Whitehouse, P. L., King, M. A., Clarke, P. J., and Bentley, M. J.: Increased ice loading in the Antarctic Peninsula since the 1850s and its effect on glacial isostatic adjustment, Geophys. Res.

Lett., 39, L17 504, doi:10.1029/2012GL052559, 2012.

Peltier, W. R.: Global glacial isostasy and the surface of the ice-age earth: the ICE5G (VM2) model and GRACE, Annu. Rev. Earth Pl. Sci., 32, 111–149, doi:10.1146/annurev.earth.32.082503.144359, 2004.

Pritchard, H. D., Ligtenberg, S. R. M., Fricker, H. A., Vaughan, D. G., van den Broeke, M. R., and Padman, L.: Antarctic ice-sheet loss driven by basal melting of ice shelves, Nature, 484, 502 – 505, doi:10.1038/nature10968, 2012.

Raymond, C. A., Ivins, E. R., Heflin, M. B., and James, T. S.: Quasi-continuous global positioning system measurements of glacial isostatic deformation in the Northern Transantarctic Mountains, Global and Planet. Change, 42, 295–303, 2004.

Rignot, E.: Changes in West Antarctic ice stream dynamics observed with ALSO PALSAR data, Geophys. Res. Lett., 35, L12 505, doi:10.1029/2008GL033365, 2008.

Rignot, E., Casassa, G., Gogineni, S., Kanagaratnam, P., Krabill, W., Pritchard, H., Rivera, A., Thomas, R., Turner, J., and Vaughan, D.: Recent ice loss from the Fleming and other glaciers, Wordie Bay, West Antarctic Peninsula, Geophys. Res. Lett., 32, L07 502, doi:10.1029/2004GL021947, 2005.

Rignot, E., Velicogna, I., van den Broeke, M. R., Monaghan, A., and Lenaerts, J.: Acceleration of the contribution of the Greenland and Antarctic ice sheets to sea level rise, Geophys. Res. Lett., 38, L05 503, doi:10.1029/2011GL046583, 2011.

Rignot, E., Bamber, J. L., Van Den Broeke, M. R., Davis, C., Li, Y., Van De Berg, W. J., and Van Meijgaard, E.: Recent Antarctic ice mass loss from radar interferometry and regional climate modelling, Nature Geosci., 1, 106–110, doi:10.1038/ngeo102, 2008.

Ritz, C., Rommelaere, V., and Dumas, C.: Modeling the evolution of Antarctic ice sheet over the last 420,000 years: Implications for altitude changes in the Vostok region, J. Geophys. Res., 106, 31,943–31,964, 2001.

Riva, R. E. M., Gunter, B. C., Urban, T. J., Vermeersen, B. L., Lindenbergh, R. C., Helsen, M. M., Bamber, J. L., van de Wal, R. S., van den Broeke, M. R., and Schutz, B. E.: Glacial Isostatic Adjustment over Antarctica from combined ICESat and GRACE satellite data, Earth Planet. Sci. Lett., 288, 516–523, doi:10.1016/j.epsl.2009.10.013, 2009.

Sasgen, I., Dobslaw, H., Martinec, Z., and Thomas, M.: Satellite gravimetry observation of Antarctic snow accumulation related to ENSO, Earth Planet. Sci. Lett., 299, 352 – 358, doi:10.1016/j.epsl.2010.09.015, 2010.

Sasgen, I., Broeke, M. v. d., Bamber, J. L., Rignot, E., Sandberg Sørensen, L., Wouters, B., Martinec, Z., Velicogna, I., and Simonsen, S. B.: Timing and origin of recent regional ice-mass loss in Greenland,

Earth Planet. Sci. Lett., 333–334, 293–303, doi:10.1016/j.epsl.2012.03.033, 2012a.

Sasgen, I., Klemann, V., and Martinec, Z.: Toward the inversion of GRACE gravity fields for present-day ice-mass changes and glacial-isostatic adjustment in North America and Greenland, J. Geodyn., 59–60, 49–63, doi:10.1016/j.jog.2012.03.004, 2012b.

Scambos, T. A., Bohlander, J. A., Shuman, C. A., and Skvarca, P.: Glacier acceleration and thinning after ice shelf collapse in the Larsen B embayment, Antarctica, Geophys. Res. Lett., 31, L18 402, doi:10.1029/2004GL020670, 2004.

Schotman, H. and Vermeersen, L.: Sensitivity of glacial isostatic adjustment models with shallow low-viscosity earth layers to the ice-load history in relation to the performance of GOCE and GRACE, Earth and Planet. Sci. Lett., 236, 828 – 844, doi:10.1016/j.epsl.2005.04.008, 2005.

Schrama, E. and Wouters, B.: Revisiting Greenland ice sheet mass loss observed by GRACE, J. Geophys. Res., 116, B02 407, doi:10.1029/2009JB006847, 2011.

Shepherd, A., Ivins, E. R., A, G., Barletta, V. R., Bentley, M. J., Bettadpur, S., Briggs, K. H., Bromwich, D. H., Forsberg, R., Galin, N., Horwath, M., Jacobs, S., Joughin, I., King, M. A., Lenaerts, J. T. M., Li, J., Ligtenberg, S. R. M., Luckman, A., Luthcke, S. B., McMillan, M., Meister, R., Milne, G., Mouginot, J., Muir, A., Nicolas, J. P., Paden, J., Payne, A. J., Pritchard, H., Rignot, E., Rott, H., Sørensen, L. S., Scambos, T. A., Scheuchl, B., Schrama, E. J. O., Smith, B., Sundal, A. V., van Angelen, J. H., van de Berg, W. J., van den Broeke, M. R., Vaughan, D. G., Velicogna, I., Wahr, J., Whitehouse, P. L., Wingham, D. J., Yi, D., Young, D., and Zwally, H. J.: A Reconciled Estimate of Ice-Sheet Mass Balance, Science, 338, 1183–1189, doi:10.1126/science.1228102, 2012.

Simms, A. R., Ivins, E. R., DeWitt, R., Kouremenos, P., and Simkins, L. M.: Timing of the most recent Neoglacial advance and retreat in the South Shetland Islands, Antarctic Peninsula: insights from raised beaches and Holocene uplift rates, Quat. Sci. Rev., 47, 41 – 55, doi:10.1016/j.quascirev.2012.05.013, 2012.

Sørensen, L. S., Simonsen, S. B., Nielsen, K., Lucas-Picher, P., Spada, G., Adalgeirsdottir, G., Forsberg, R., and Hvidberg, C. S.: Mass balance of the Greenland ice sheet (2003–2008) from ICESat data - the impact of interpolation, sampling and firn density, The Cryosphere, 5, 173–186, doi:10.5194/tc-5-173-2011, 2011.

Tarantola, A.: Inverse Problem Theory and Methods for Model Parameter Estimation, Society for Industrial and Applied Mathematics, Philadelphia, 2005.

Thomas, I. D., King, M. A., Bentley, M. J., Whitehouse, P. L., Penna, N. T., Williams, S. D. P., Riva, R. E. M., Lavallee, D. A., Clarke, P. J., King, E. C., Hindmarsh, R. C. A., and Koivula, H.: Widespread low rates of Antarctic glacial isostatic adjustment revealed by GPS observations, Geophys. Res. Lett.,

Table 1. Upper and lower mantle viscosity values (Pa s) for the four applied viscosity distributions.

	VD1	VD2	VD3	VD4
η_{UM}	$4{\cdot}10^{20}$	$2{\cdot}10^{20}$	$6{\cdot}10^{20}$	$8{\cdot}10^{20}$
η_{LM}	$2{\cdot}10^{21}$	$5{\cdot}10^{21}$	$2{\cdot}10^{22}$	$4{\cdot}10^{22}$

38, L22 302, doi:10.1029/2011GL049277, 2011.

Velicogna, I.: Increasing rates of ice mass loss from the Greenland and Antarctic ice sheets revealed by GRACE, Geophys. Res. Lett., 36, L19 503, doi:10.1029/2009GL040222, 2009.

Velicogna, I. and Wahr, J.: Measurements of Time-Variable Gravity Show Mass Loss in Antarctica, Science, 311, 1754–1756, doi:10.1126/science.1123785, 2006.

Whitehouse, P. L., Bentley, M. J., and Brocq, A. M. L.: A deglacial model for Antarctica: geological constraints and glaciological modelling as a basis for a new model of Antarctic glacial isostatic adjustment, Quat. Sci. Rev., 32, 1 – 24, doi:10.1016/j.quascirev.2011.11.016, 2012a.

Whitehouse, P. L., Bentley, M. J., Milne, G. A., King, M. A., and Thomas, I. D.: A new glacial isostatic adjustment model for Antarctica: calibrated and tested using observations of relative sea-level change and present-day uplift rates, Geophys. J. Int., 190, 1464–1482, doi:10.1111/j.1365-246X.2012.05557.x, 2012b.

Wu, P., Steffen, H., and Wang, H.: Optimal locations for GPS measurements in North America and northern Europe for constraining Glacial Isostatic Adjustment, Geophys. J. Int., 181, 653–664, doi:10.1111/j.1365-246X.2010.04545.x, 2010.

Wu, X., Heflin, M. B., Schotman, H., Vermeersen, B. L. A., Dong, D., Gross, R. S., Ivins, E. R., Moore, A. W., and Owen, S. E.: Simultaneous estimation of global present-day water transport and glacial isostatic adjustment, Nature Geosci., 3, 642–646, 2010.

Yegorova, T., Bakhmutov, V., Janik, T., and Grad, M.: Joint geophysical and petrological models for the lithosphere structure of the Antarctic Peninsula continental margin, Geophys. J. Int., 184, 90–110, doi:10.1111/j.1365-246X.2010.04867.x, 2011.

Zwally, H. and Giovinetto, M.: Overview and Assessment of Antarctic Ice-Sheet Mass Balance Estimates: 1992-2009, Surv. Geophys., 32, 351–376, doi:10.1007/s10712-011-9123-5, 2011.

Zweck, C. and Huybrechts, P.: Modelling the Northern Hemisphere ice sheet during the last glacial cycle and glaciological sensitivity, J. Geophys. Res., 110, D07 103, 2005.

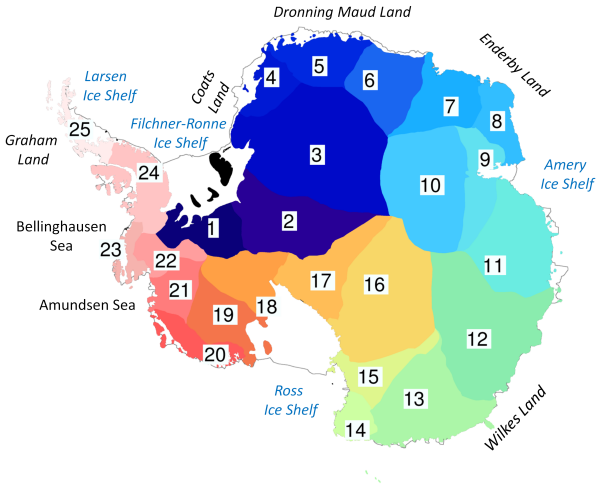

Fig. 1. Division of 25 Antarctic drainage basins investigated in this study (after Rignot et al., 2008; Zwally and Giovinetto, 2011)

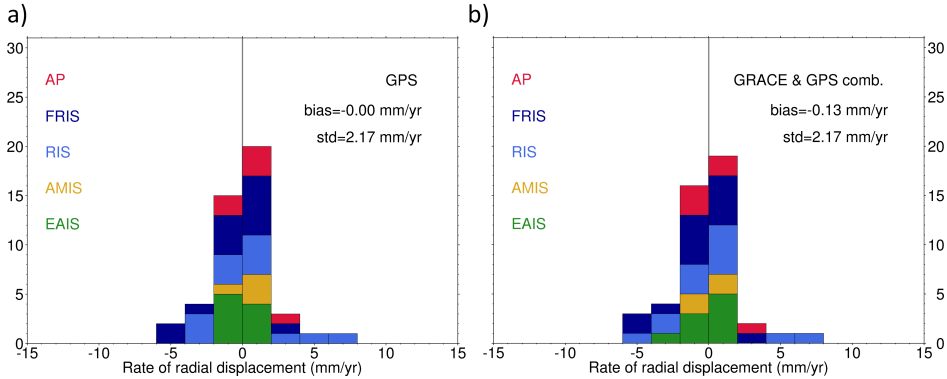

Fig. 2. Observed minus predicted rate of surface deformation at GPS sites. Shown are the residuals in GPS-measured (mean of InSAR and ICESat-based elastic and Northern Hemisphere GIA correction applied) minus GIA estimated uplift rates, based on GPS (left) and GRACE&GPS observations (right). Residuals <0 (>0) indicate overestimated (underestimated) GIA with respect to the GPS uplift rates. The residuals are separated for each sector, Antarctic Peninsula (AP; red), Filchner-Ronne Ice Shelf (FRIS; dark blue), Ronne Ice Shelf (RIS; light blue), Amery Ice Shelf (AMIS; yellow) and the remaining parts, East Antarctica (EAIS; green). Also indicated are the mean bias (bias; not weighted), as well as the standard deviation (std; not weighted).

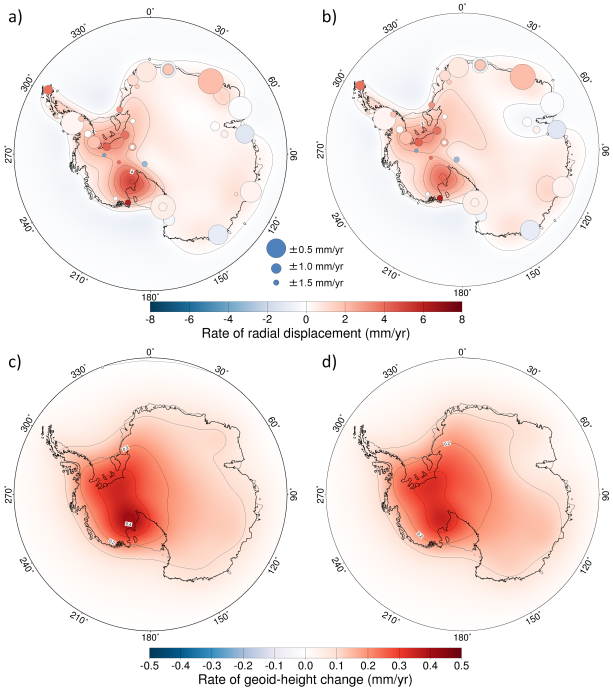

Fig. 3. B8 Rate of radial displacement and geoid-height change (mm/yr) for the GIA estimate a) and c) AGE1 (GPS only) and b) and d) AGE1 (GPS&GRACE), respectively. Spherical-harmonic cut-off degrees are 0 to 170 for a) and b) and 2 to 60 for c) and d). Also indicated are the GPS uplift rates (after the correction for the Northern Hemisphere contribution) according Thomas et al. (2011)

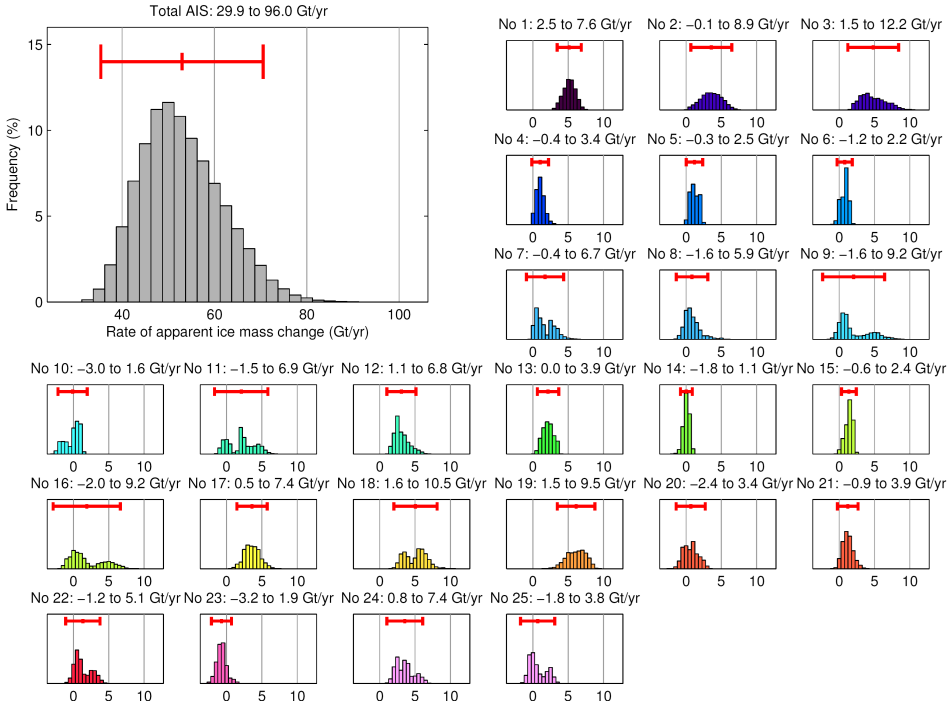

Fig. 4. Distribution of the rate of apparent ice-mass change (Gt/yr) induced by the GIA for the total AIS and the 25 basins, obtained by constraining the ensemble of per-sector combinations (995328 samples) with GPS and GRACE (GRACE & GPS comb.). The apparent ice-mass change is calculated by applying the gravimetric inversion method for the present-day ice-mass changes to each estimate of the GIA-induced gravity field.

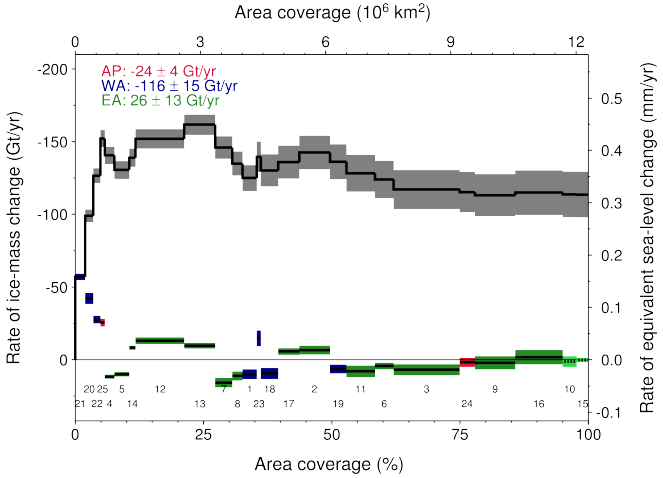

Fig. 5. Rate of basin-scale ice-mass change from GRACE (Gt/yr) for the drainage basins of the Antarctic Peninsula (red), West Antarctica (blue) and East Antarctica (green). Numbers in the bottom part of the plot refer to the drainage basins in Figure 1 and Table 2. Grey bars reflect 1-sigma uncertainties. The drainage basins are sorted according to the estimated signal-to-noise ratio of the linear trend component. GIA correction AGE1 (GRACE&GPS) applied. Statistically insignificant temporal components are indicated with a dashed lines. The cumulative sum over the basins is provided in the top part of the Figure, depicting that nearly all mass loss originates from a very small portion of the AIS.

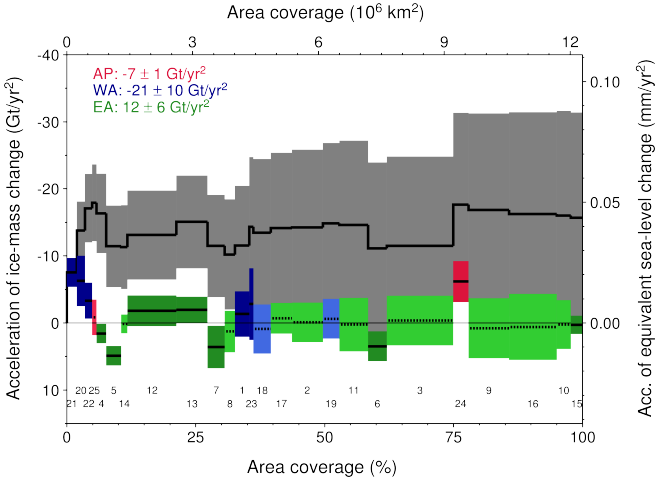

Fig. 6. Same as 5, but the acceleration of basin-scale ice-mass change (Gt/yr^2)

Table 2. Rate and acceleration of basins-scale ice-mass change from GRACE and revised GIA estimate AGE1. The GRACE estimates represent error-weighted values of GFZ RL05 and CSR RL05 estimates. $*$ denotes statistical significant acceleration terms in both GFZ RL05 and CSR RL05, while $\diamondsuit$ denotes linear trends that not statistically significant in both releases (95% confidence interval; before correcting for GIA). Time period is January 2003 to September 2012.

Drainage basin	Area (10^3km^2)	GRACE (GIA corr.) $\dot{m}$	GRACE $\ddot{m}$	GIA (GRACE+GPS) $\dot{m}$	GIA (GPS only) $\dot{m}$	GRACE (no GIA corr.) $\dot{m}$
24	369	2±4	-6±1	4±3	3±3	5±2
25	104	-26±3	-1±1	1±2	0±2	-25±1
Ant. Peninsula	473	-24±4	-7±1	4±4	4±3	-20±3
1	342	10±7	-1±5	5±2	5±2	15±7
18	414	9±5	1±4	5±3	4±3	15±4
19	391	6±4	-1±1	6±3	5±3	13±2
20	195	-42±5	-6±6*	1±2	1±2	-41±4
21	235	-57±3	-8±1*	1±1	1±1	-56±3
22	175	-28±3	-3±1*	1±2	1±2	-26±2
23	96	-15±9	-3±5	-1±1	-1±1	-15±8
West Ant.	1848	-116±15	-21±10	19±6	16±6	-97±13
2	738	-7±3	-0±1	4±3	4±3	-3±0
3	1582	7±4	-0±1	5±4	5±5	12±1
4	226	12±1	2±1*	1±1	1±1	13±1
5	361	10±1	5±1*	1±1	1±1	11±1
6	443	4±3	3±2*	1±1	1±1	5±3
7	412	16±4	4±3*	2±3	1±2	17±2
8	243	11±3	1±1	1±2	0±2	12±3
9	963	2±5	1±1	2±4	2±5	4±1
10	335	1±4	0±1	-0±2	-1±3	1±4$^\diamondsuit$
11	690	8±4	0±2	2±4	2±5	10±1
12	1170	-13±2	-2±1*	3±2	4±3	-10±1
13	741	-10±2	-2±1*	2±2	3±2	-8±1
14	147	-8±2	0±1	0±1	0±1	-8±1
15	281	0±2	0±1	1±1	1±1	1±2$^\diamondsuit$
16	1138	-2±5	1±1	2±5	2±6	0±2$^\diamondsuit$
17	506	-6±2	-1±2	4±2	3±2	-2±1
East Ant.	9976	26±13	12±6	30±11	30±13	56±7
Total AIS	12297	-114±23	-16±12	53±18	50±26	-61±15